Time-dependent growth of nuclear spin polarization under periodic optical pumping

Michael J. Dominguez [1] Hua-Wei Hsu [1] and Vanessa Sih [2,*]

[1]*Applied Physics Program, University of Michigan, Ann Arbor, Michigan 48109, USA*
[2]*Department of Physics, University of Michigan, Ann Arbor, Michigan 48109, USA*

Consecutive circularly polarized optical pulses generate and rotate electron spin polarization through optical orientation and the optical Stark effect. We perform time- and magnetic-field-dependent optical pump-probe measurements on gallium arsenide and observe a variable Overhauser field growth that depends on the external magnetic field and laser wavelength. We show that the time dependence of the nuclear spin polarization can be attributed to the time-averaged electron spin polarization produced along the external magnetic field direction.

I. INTRODUCTION

The manipulation of electron and nuclear spin polarization in solids is of interest for potential applications in both classical and quantum information processing. Under certain conditions, the nuclear spin polarization time can exceed the electron spin coherence time, providing a reservoir to store information beyond the electron spin coherence time [1–3].

Nuclear-induced frequency focusing (NIFF) has been observed and theoretically modelled in periodic optical electron spin pumped semiconductor quantum dots and epilayers [4–10]. The nuclear spin polarization changes to maintain plateaus with discrete values of Larmor precession frequency that depend on the repetition rate of the periodic optical pumping. This has been attributed to the optical Stark effect from detuning from the trion excitation energy. Previous optical pump-probe experiments have investigated the relationship between the spectral detuning from resonance of the periodic optical excitation and the induced nuclear polarization produced by NIFF [11,12]. In our previous work, we also presented numerical simulations of the nuclear polarization produced by different optical pump spectral detunings from the trion resonance and applied magnetic field history [12].

Measurements of the nuclear polarization build-up dynamics in semiconductors have been performed with optical pump-probe and other techniques [13–17]. These experiments were not performed under conditions where the NIFF effect would occur, and the nuclear spin polarization is shown to change exponentially, with a saturation change in the nuclear field and a single characteristic saturation time.

In this article, we show that under conditions that produce NIFF, the nuclear polarization time and build-up characteristics sensitively depend on the external magnetic field and pump wavelength detuning from the trion resonance. We numerically calculate and measure the Overhauser field growth as a function of time for various magnetic fields and spectral detunings under periodic optical pumping in the Voigt geometry. We present experimental time-resolved Kerr rotation (TRKR) measurements, where, by taking successive data points at fixed external fields and pump-probe delays, the Overhauser field build-up behavior for different external fields and spectral detunings is extracted. Observations from both the experimental and simulated data demonstrate drastically different nuclear polarization build-up behavior between positive and negative detuning. The difference in build-up behavior is most noticeable at magnetic fields near the NIFF boundaries. In the case of positive detuning, the nuclear polarization build up does not appear to exhibit monoexponential growth behavior. Our calculations and measurements show that under the conditions where the NIFF effect is present, the nuclear polarization build-up behavior changes over time due to the changing magnitude of the time-averaged electron spin polarization produced along the external magnetic field direction.

II. MODEL

The coupled dynamics of the electron and nuclear spin systems under periodic pumping in the Voigt geometry are calculated using the model outlined in Ref. [12]. This model is equivalent to the one implemented in Ref. [8].

Optically oriented electrons in GaAs couple to the nuclear spin system through the Fermi contact term of the hyperfine interaction [18]. In the presence of an external magnetic field, the contact hyperfine interaction has been shown to polarize the nuclear spin system along the direction of the external magnetic field. The rate at which the nuclear spin polarization changes can be described by the following rate equation:

$$\frac{dI_{av}}{dt} = -\frac{1}{T_{1e}}\left[I_{av} - \frac{4}{3}I(I+1)\langle S_x\rangle\right] - \frac{I_{av}}{T_{1n}}, \qquad (1)$$

where I_{av} is the nuclear spin polarization and $\langle S_x\rangle$ is the time-averaged electron spin component along the magnetic field [18,19]. The variable I is the nuclear spin number, T_{1e} is the nuclear spin polarization time due to the hyperfine interaction with electron spins, and T_{1n} is the nuclear spin polarization time due to other mechanisms. From Eq. (1), we see that the
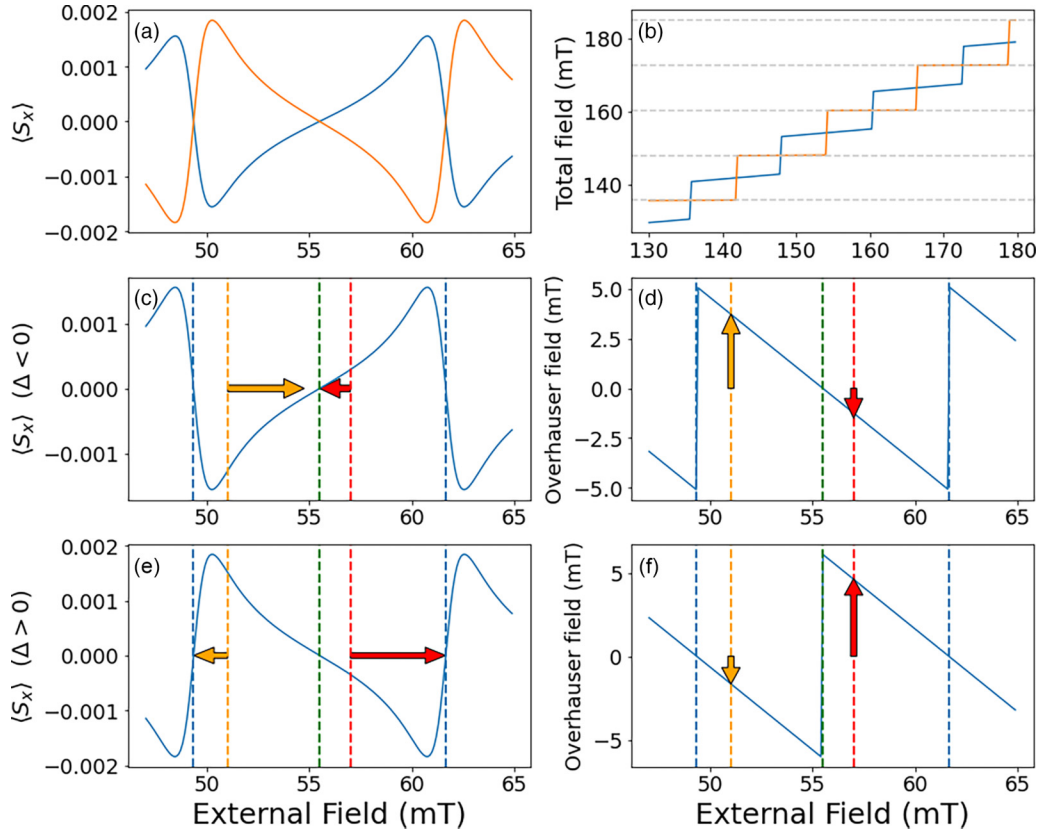
*vsih@umich.edu

FIG. 1. Relationship between $\langle S_x \rangle$ and steady-state Overhauser field. (a) Calculated time-averaged $\langle S_x \rangle$ component for negative detuning (819.5 nm) in blue and positive detuning (818.2 nm) in orange. (b) Simulated steady-state total effective magnetic field for both detunings, showing that the positive detuning (orange) results in integer multiples of $\frac{h}{g\mu_B T_{\text{rep}}}$, denoted by the gray dashed horizontal lines, while the negative detuning (blue) exhibits plateaus at the half-integer values. (c)–(f) The blue and green vertical lines correspond to the integer and half-integer values, respectively. The orange and red vertical lines are example external fields, and the orange and red arrows demonstrate the magnitude and direction the Overhauser field builds for the total field to reach the integer or half-integer values.

rate in polarization is directly dependent on $\langle S_x \rangle$. The nuclear spin polarization will produce an Overhauser field $\vec{B}_N$ that acts on the electrons,

$$\vec{B}_N = bn * I_{av}[t, \langle S_x(B_{\text{tot}}) \rangle] \hat{x},$$

$$bn = \sum_i \frac{A_i \chi_i}{\mu_B g}.$$

Here, χ_i is the abundance of nuclear spin species, A_i is the hyperfine coupling constant, g is the g factor, and μ_B is the Bohr magneton [20]. The value bn is the conversion factor between the nuclear polarization and Overhauser field.

The Overhauser field contributes to the total magnetic field B_{tot} and will alter the effective Larmor precession frequency experienced by the electrons,

$$\Omega_{\text{tot}} = \frac{g\mu_B}{\hbar} B_{\text{tot}} = \frac{g\mu_B}{\hbar} (B_{\text{ext}} + B_N).$$

Our experiments are performed in the Voigt geometry where the external magnetic field is along the x direction and perpendicular to the optical axis and direction of the optical spin generation, z. However, the arrival of a subsequent pump pulse can rotate spin polarization to be along the magnetic field due to the optical Stark effect [11,12].

The average spin component $\langle S_x \rangle$ is dependent on the effective Larmor precession. This consequently leads to coupling and dynamic feedback between the spin systems through the Overhauser field. The dynamics of the nuclear polarization, described in Eq. (1), are nonlinear and further complicated by the Overhauser field feedback between the spin systems. The steady-state nuclear polarization can be solved by setting the left-hand side of Eq. (1) to zero,

$$I_{av} = \left(\frac{T_{1n}}{T_{1n} + T_{1e}} \right) \frac{4}{3} I(I+1) \langle S_x \rangle. \tag{2}$$

The steady-state form of I_{av} is transcendental through its dependence on $\langle S_x \rangle$. A closed-form expression of $\langle S_x \rangle$ from periodic pumping and its dependence on spectral detuning from the trion resonance, $\Delta = (E_{\text{pump}} - E_t)\tau_p/2\pi\hbar$, can be found in Ref. [11]. In this expression, E_{pump} is the energy of the pump laser, E_t is the trion resonance energy, τ_p is the pump pulse duration, and $\hbar$ is the reduced Planck's constant. Calculations of $\langle S_x \rangle$ and the steady-state Overhauser field as a function of applied magnetic field for both positive and negative spectral detuning are shown in Fig. 1. The external field dependence of $\langle S_x \rangle$, neglecting the Overhauser field, for both negative and positive detuning is shown in Fig. 1(a).

The total magnetic field shown in Fig. 1(b) is calculated from the steady-state Overhauser field using Eq. (2) and

the external field. The coupling between $\langle S_x \rangle$ and I_{av} leads to the total magnetic field exhibiting steplike features, with plateaus appearing near integer (or half-integer) multiples of $\frac{h}{g\mu_B T_{rep}}$ for positive (or negative) spectral detuning. This effect is nuclear-induced frequency focusing (NIFF), where the value corresponds to synchronization with the laser's pulse repetition period (T_{rep}) [4]. The laser repetition period and electron spin g factor in our experiments are 13.16 ns and -0.44, respectively. This yields a value for the factor $\frac{h}{g\mu_B T_{rep}} \approx -12.3$ mT.

In the case of a long T_{1n} relaxation time, the first term of the rate equation (1) and the dependence of I_{av} in Eq. (2) suggest that both I_{av} and $\langle S_x \rangle$ will change until $\langle S_x \rangle$ reaches a value of zero. For both positive and negative spectral detuning, the component $\langle S_x \rangle$ is zero only at external field values corresponding to integer and half-integer multiples of $\frac{h}{g\mu_B T_{rep}}$. In Figs. 1(c) and 1(e), these external fields are marked by the dashed blue and green vertical lines. For the case of negative detuning shown in Fig. 1(c), the orange vertical line corresponds to an initial external field slightly above an integer multiple of $\frac{h}{g\mu_B T_{rep}}$. At this detuning and external field, the $\langle S_x \rangle$ component is negative in sign, which leads to a positive increase of the Overhauser field. This is due to the conversion constant (bn) having a negative value in GaAs. The increasing Overhauser field will continue to increase the total magnetic field until it equals the half-integer multiple of $\frac{h}{g\mu_B T_{rep}}$, where the $\langle S_x \rangle$ component is zero. In this example, the corresponding Overhauser field reaches a value of approximately 4 mT, as represented by the orange arrows in Figs. 1(c) and 1(d).

The red dashed vertical line corresponds to the case of setting the initial field to slightly higher than the half-integer value. For this initial external field, the $\langle S_x \rangle$ component is positive in sign. Thus, the Overhauser field is negative in value and decreases the total magnetic field, which also results in the total magnetic field reaching an integer-and-a-half multiple value of $\frac{h}{g\mu_B T_{rep}}$. This steady-state Overhauser field shift is represented by red arrows in Figs. 1(c) and 1(d).

For the case of positive detuning, the $\langle S_x \rangle$ component is opposite in sign. Using the same intuition of the relationship between the sign of $\langle S_x \rangle$ and the Overhauser field magnitude, we illustrate the growth and direction of the total magnetic field. In Figs. 1(e) and 1(f), we see that for positive detuning, the total magnetic field is pushed to values of integer $\frac{h}{g\mu_B T_{rep}}$, represented by the blue dashed vertical lines.

The $\langle S_x \rangle$ dependence on the external field can be described as periodic, with a period of $\frac{h}{g\mu_B T_{rep}}$ and crossing zero at half this period. Since $\langle S_x \rangle$ is flipped in sign between positive and negative detuning, and not merely a half-wavelength shift, this implies that nuclear polarization growth will be different between positive and negative detuning. Qualitatively, this difference in polarization behavior can be described with features seen in Figs. 1(c) and 1(e), where the initial fields at the orange and red vertical lines are examples where the Overhauser field builds to nearly its largest magnitude for negative and positive detuning, respectively.

In Fig. 1(c), at the initial external field of the orange vertical line, the initial $\langle S_x \rangle$ component is nearly at its largest magnitude. This leads to an initial rapid build in nuclear polarization, as described by Eq. (1). As this nuclear polarization builds and increases the total magnetic field, the $\langle S_x \rangle$ component decreases steadily, which leads to a slower rate of change in polarization.

For the positive detuning example in Fig. 1(e), the initial $\langle S_x \rangle$ component at the external field of the red dotted line is of a small magnitude. This leads to an initial slow building of the nuclear polarization. As the Overhauser field builds in magnitude and increases the total effective magnetic field, the magnitude of $\langle S_x \rangle$ increases slowly at first and then more rapidly before decreasing again as the total effective magnetic field approaches an integer multiple of $\frac{h}{g\mu_B T_{rep}}$.

We calculate this behavior by numerically integrating Eq. (1) with respect to time for positive and negative detunings and different external magnetic fields. The initial nuclear polarization is set to zero for each integration. The results of these calculations are plotted in Fig. 2, where the qualitatively described growth behaviors can be seen.

The calculations for negative detuning are shown in Figs. 2(a) and 2(b). For the polarization behavior of initial external fields in the vicinity of the NIFF boundary, in Fig. 2(a), we can observe the rapid initial rate of polarization followed by slower growth to their steady-state values over time. Figure 2(b) shows the Overhauser field plotted as a function of external magnetic field for different elapsed times.

The calculated polarization behavior for positive detuning is shown in Figs. 2(c) and 2(d). For initial external fields near the NIFF boundaries, the rate of polarization initially is slow in comparison to the rate of polarization for negative detuning. These rates of polarization grow logistically over time, where there is an inflection point of rapid change followed by a slow approach to the steady-state value. This inflection point corresponds to the total effective field reaching the value at which the absolute magnitude of $\langle S_x \rangle$ reaches its maximum value. Figure 2(d) shows how the Overhauser field as a function of external magnetic field changes with elapsed time for positive detuning.

III. 2D KERR EXPERIMENTS

Optical pump-probe measurements of electron spin polarization are performed in order to monitor the change in the Larmor precession frequency and Overhauser field over time. The measurements are conducted at different applied magnetic fields and for both negative and positive detuning in order to see whether the simulated Overhauser field growth profiles are reproduced.

The experimental data presented in this paper were collected on a 2-μm-thick Si-doped n-type GaAs epilayer with a carrier concentration of $n = 3 \times 10^{16}$ cm^{-3} at $T = 10$ K. The n-GaAs layer was grown by molecular-beam epitaxy on a 1-μm-thick undoped AlGaAs layer, which was grown on a 635-μm-thick undoped GaAs substrate. The photoluminescence spectrum for this sample is shown in Ref. [21] and is similar to the spectrum for the GaAs sample shown in Ref. [22].

A Ti:sapphire laser is used to optically generate and detect electron spin polarization in the GaAs sample. The Ti:sapphire laser is mode locked and outputs pulses with a 2-ps temporal width every 13.16 ns, which corresponds to
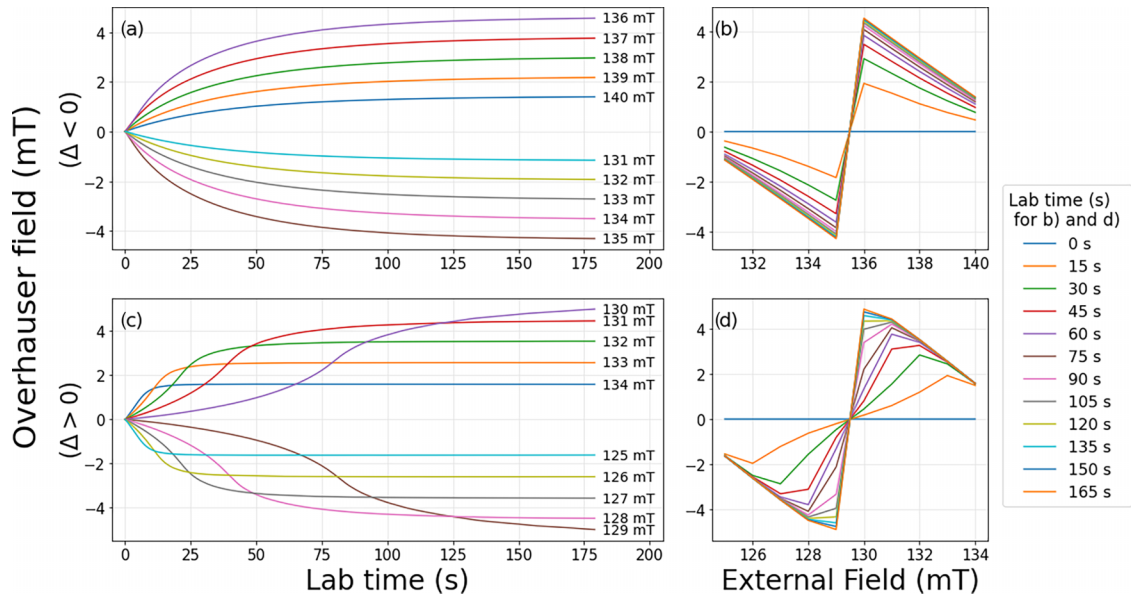
FIG. 2. Simulated Overhauser field growth profiles for different external field values and (a) negative detuning and (c) positive detuning. Each curve is labeled with its external magnetic field value. In the case of positive detuning, we observe that the curves for 129 and 130 mT result in the largest Overhauser fields, but have an initial slow delayed growth before the Overhauser field increases more rapidly. (b), (d) The Overhauser field profile plotted as a function of external field for different elapsed laboratory times.

a repetition frequency of 76 MHz. In the experiments, the time-resolved Kerr rotation (TRKR) measurement scheme is used, in which a pump laser pulse excites an electron spin polarization, and a time-delayed probe laser pulse measures the electron spin polarization. Since the same Ti:sapphire laser provides both the pump and probe beams for our experiments, the pump and probe have the same wavelength. The pump beam is sent through a photoelastic modulator, which modulates the pump polarization between left and right circular polarization, and the probe beam is modulated by an optical chopper at a frequency of 1.37 kHz. After reflecting off the sample, the probe beam passes through a Wollaston prism, which splits the reflected probe into two components linearly polarized at $+45°$ and $-45°$ with respect to the initial probe polarization. The intensity difference between the two components is recorded and processed by two cascaded lock-in amplifiers at the photoelastic modulator and optical chopper frequencies, and the Kerr rotation signal is measured.

In order to experimentally characterize the nuclear spin polarization as a function of the laser wavelength, external magnetic field, and laboratory time, the following measurement scheme is used. We first fix the time delay between the pump and probe beams at a fixed external field. Kerr rotation measurements are performed at intervals of approximately 1.1 s for a duration of 1 to 3 minutes, which results in a total of 60 to 180 data points. During this time, the nuclear field is allowed to build up under the specific combination of the pump-probe delay time and the external field. After performing Kerr rotation measurements over this duration, the time delay between the pump and probe beams is changed by an interval of $+200$ ps. Subsequently, Kerr rotation measurements are performed again for the same duration under the same external field at the new delay time. The measurement procedure is followed until all delay time indices from 0 to 5000 ps are traversed, which results in 2D Kerr rotation data

in which the axes are laboratory time and pump-probe delay time. At the beginning of every delay time increment, we temporarily set the external field to 0 mT for 15 s. This ensures that the nuclear spin system is depolarized at the start of every 1 to 3 minute duration of Kerr rotation measurements.

The 2D Kerr rotation data for positive detuning and 133 mT external field are shown in Fig. 3(a), where the vertical axis is the pump-probe delay time and the horizontal axis is the laboratory time over the 1 to 3 minute duration over which the Kerr rotation measurements are taken. The color of the 2D plot corresponds to the Kerr rotation value in arbitrary units. Since the nuclei are initially depolarized and the nuclear spin polarization grows on the scale of minutes, each vertical slice of the data allows us to view Kerr rotation measurements for different pump-probe delay times, affected by the same amount of nuclear polarization at a given laboratory time. Vertical slices of the data for different laboratory times are plotted in Fig. 3(b), where we can see the change in Larmor precession frequency of the electron spin polarization for increasing laboratory times. This change in Larmor precession frequency is due to the building Overhauser field from the nuclear polarization. As the total magnetic field felt by the electron spins is the sum of the external field and the Overhauser field, the laboratory time-dependent magnitude of the Overhauser field can be inferred by the change in Larmor precession frequency.

IV. EXTRACTING OVERHAUSER FIELD GROWTH

By curve fitting the vertical slices of the 2D Kerr data to a decaying cosine, $Ae^{-\Delta t/\tau} \cos(\Omega \Delta t + \phi)$, we extract the Larmor precession frequency as a function of laboratory time. These 2D Kerr measurements are repeated for different applied external fields for both positive and negative spectral detuning. The positive detuning measurements are conducted
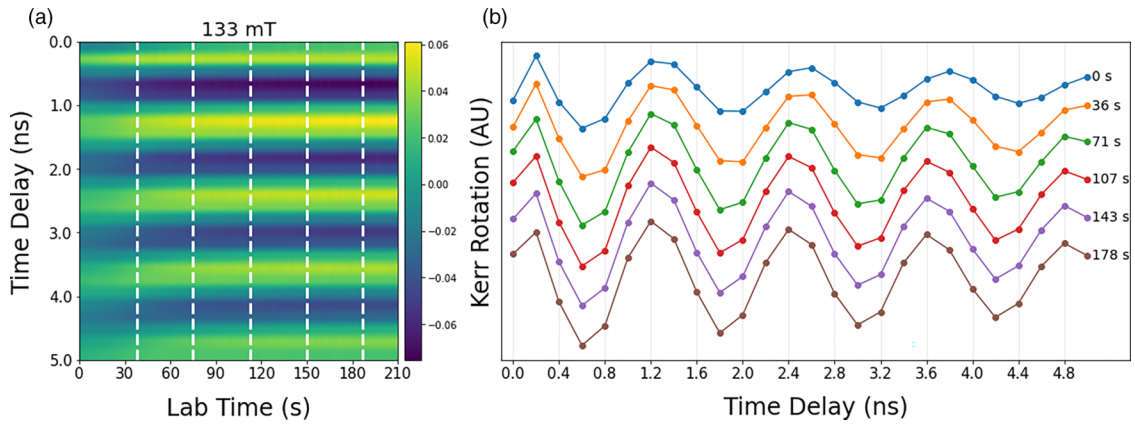
FIG. 3. Two-dimensional (2D) Kerr data and plots of Kerr rotation as a function of time delay for different laboratory times. (a) Experimental 2D TRKR data for external field of 133 mT and wavelength of 818.2 nm. The vertical axis is the pump-probe delays, and the horizontal axis is the laboratory time. (b) TRKR data at select laboratory times plotted with respect to the pump-probe time delay. The data correspond to vertical slices of the 2D data, denoted by the vertical white dashed lines in (a).

at 818.2 nm, and the negative detuning measurements are conducted at 819.5 nm. The fits of Larmor frequency for all fields and laboratory times and both detunings are summarized in Fig. 4. Figure 4(a) shows the change in Larmor frequency for negative detuning. We observe that the Larmor frequency changes over laboratory time and approaches the integer multiples of either 10.5 or 11.5 of $n * 2\pi/T_{rep}$, depending on whether the initial Larmor frequency is less than or greater than 11 times $2\pi/T_{rep}$. Figure 4(c) shows the change in Larmor frequency for positive detuning. For the initial external field values whose Larmor frequencies lie in the center

between the multiples of $2\pi/T_{rep}$, we see the growth behavior predicted in Fig. 2(c), where the change in precession is slow at first and then rapidly increases and then saturates. This inflection point in the rate of change approximately corresponds to where the total effective magnetic field results in the largest $\langle S_x \rangle$ magnitude. In Figs. 4(b) and 4(d), we observe that the Larmor frequency approaches the half-integer or integer multiples of $n * 2\pi/T_{rep}$, as shown in Fig. 1(b).

Note the growth curves for 131.5 mT in Fig. 4(c), where the Larmor frequency drifts but does not reach the integer multiple values of $2\pi/T_{rep}$. This is due to the instability of
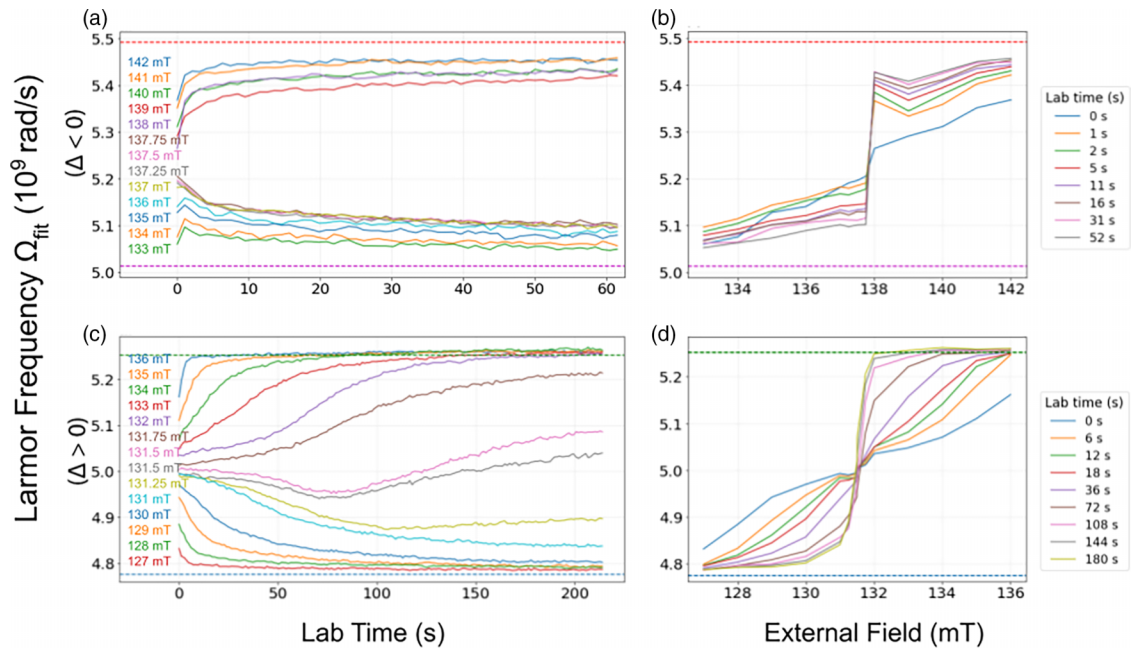

FIG. 4. Larmor frequency curve fits for all laboratory times, different external fields, and both spectral detunings. (a), (b) Larmor frequencies for negative detuning. The magenta and red horizontal dashed lines correspond to the predicted NIFF half-integer values of 10.5 and 11.5 of $n * 2\pi/T_{rep}$. The Larmor frequency rapidly changes to approach one of these half-integer values depending on the external field. (c), (d) Larmor frequencies for positive detuning. The blue and green horizontal dashed lines correspond to the predicted NIFF integer values of 10 and 11 of $n * 2\pi/T_{rep}$. The predicted delayed growth behavior for fields with a larger predicted Overhauser field is observed.

nuclear polarization for this region for positive detuning. We observe that this region has the smallest magnitude and slope of $\langle S_x \rangle$ with respect to the field [Fig. 1(e)]. This leads to both the slowest rate and change in rate of nuclear polarization. The observed drift in Larmor precession may be due to small fluctuations in the external field crossing over the unstable point. We remeasured data for 131.5 mT and observed similar but not identical behavior, as shown in Fig. 4(c).

V. CONCLUSION

We have numerically simulated and experimentally measured how the Overhauser field changes in a system that exhibits nuclear-induced frequency focusing. The Overhauser field changes in response to the changing magnitude of the electron spin polarization and, thus, does not exhibit a single characteristic saturation time. In the case of positive spectral detuning and external magnetic field further from the NIFF boundaries, the rate of change of the Overhauser field increases as the total effective magnetic field approaches the NIFF boundaries, and we show that this behavior can be observed in both the numerical simulations and from 2D Kerr measurements.

The numerical results were calculated using an iterative model to determine the electron and nuclear spin polarization and assumes an Overhauser field distribution produced by the spectral distribution of the laser pulses used in the experiment [12]. Other sources of inhomogeneity that are potentially present in the experiment, such as variation in the external magnetic field over time, are not accounted for in the simulation and could be responsible for the slightly different behavior measured at 131.5 mT for positive detuning in Fig. 4(c). Physical parameters of the model such as the T_1 and T_2 times are chosen to qualitatively demonstrate the behavior of the experimental results and are consistent with previously reported values [13,14]. As shown in Fig. 4(c), some of the data do not reach their steady-state values within 200 s. The numerical results shown in Fig. 2 assumed $T_{1e} = 400$ s, $T_{1n} = 600$ s, $T_2 = 30$ ns, power area $\theta = \pi/4$, and 50 discrete bins for nuclear polarization spanning an inhomogeneous pump wavelength with a standard deviation of 0.6 nm [12].

The model presented here assumes a constant value for the nuclear spin polarization times. This model could be extended to take into account a changing T_{1e} that depends on the Overhauser field and the applied magnetic field, as discussed in Ref. [23]. However, the model with constant nuclear spin polarization times already reproduces many features of the experimental data shown in Fig. 4. For example, in Fig. 2(a), for the case of negative detuning, the Overhauser field increases monotonically and reaches a larger magnitude for external fields that are in the middle of the range of the shown magnetic fields, and, in Fig. 2(b), for the case of positive detuning, the growth rate of the Overhauser field is different for different external fields and exhibits regions of slower and faster growth over time.

We have experimentally observed and extracted the laboratory time-dependent growth of the nuclear polarization as it approaches the magnetic field plateaus produced by NIFF. These observations are corroborated by numerical calculations. We show that the growth behavior for both positive and negative detuning is determined by the $\langle S_x \rangle$ magnitude. We also demonstrated an experimental TRKR measurement technique in which the laboratory time-dependent nuclear polarization growth can be directly inferred.

[1] D. R. McCamey, J. Van Tol, G. W. Morley, and C. Boehme, Electronic Spin storage in an electrically readable nuclear spin memory with a lifetime >100 seconds, Science **330**, 1652 (2010).

[2] J. P. King, Y. Li, C. A. Meriles, and J. A. Reimer, Optically rewritable patterns of nuclear magnetization in gallium arsenide, Nat. Commun. **3**, 918 (2012).

[3] D. A. Gangloff, G. Ethier-Majcher, C. Lang, E. V. Denning, J. H. Bodey, D. M. Jackson, E. Clarke, M. Hugues, C. Le Gall, and M. Atature, Quantum interface of an electron and a nuclear ensemble, Science **364**, 62 (2019).

[4] A. Greilich, A. Shabaev, D. R. Yakovlev, Al. L. Efros, I. A. Yugova, D. Reuter, A. D. Wieck, and M. Bayer, Nuclei-induced frequency focusing of electron spin coherence, Science **317**, 1896 (2007).

[5] S. Markmann, C. Reichl, W. Wegscheider, and G. Salis, Universal nuclear focusing of confined electron spins, Nat. Commun. **10**, 1097 (2019).

[6] E. Evers, N. E. Kopteva, I. A. Yugova, D. R. Yakovlev, D. Reuter, A. D. Wieck, M. Bayer, and A. Greilich, Suppression of nuclear spin fluctuations in an InGaAs quantum dot ensemble by GHz-pulsed optical excitation, npj Quantum Inf. **7**, 60 (2021).

[7] E. A. Zhukov, E. Kirstein, N. E. Kopteva, F. Heisterkamp, I. A. Yugova, V. L. Korenev, D. R. Yakovlev, A. Pawlis, M. Bayer, and A. Greilich, Discretization of the total magnetic field by the nuclear spin bath in fluorine-doped ZnSe, Nat. Commun. **9**, 1941 (2018).

[8] N. E. Kopteva, I. A. Yugova, E. A. Zhukov, E. Kirstein, E. Evers, V. V. Belykh, V. L. Korenev, D. R. Yakovlev, M. Bayer, and A. Greilich, Theoretical modeling of the nuclear-field induced tuning of the electron spin precession for localized spins, Phys. Stat. Solidi B **256**, 1800534 (2019).

[9] P. Schering, J. Hudepohl, G. S. Uhrig, and B. Fauseweh, Nuclear frequency focusing in periodically pulsed semiconductor quantum dots described by infinite classical central spin models, Phys. Rev. B **98**, 024305 (2018).

[10] P. Schering, P. W. Scherer, and G. S. Uhrig, Interplay of spin mode locking and nuclei-induced frequency focusing in quantum dots, Phys. Rev. B **102**, 115301 (2020).

[11] M. J. Dominguez, J. R. Iafrate, and V. Sih, Dynamic nuclear polarization by optical Stark effect in periodically pumped gallium arsenide, Phys. Rev. B **101**, 205203 (2020).

[12] M. J. Dominguez, J. R. Iafrate, and V. Sih, Nuclear-induced frequency focusing and Overhauser field distributions in periodically pumped gallium arsenide, Phys. Rev. B **104**, 235204 (2021).

[13] J. M. Kikkawa and D. D. Awschalom, All-optical magnetic resonance in semiconductors, Science **287**, 473 (2000).

[14] D. Kölbl, D. M. Zumbuhl, A. Fuhrer, G. Salis, and S. F. Alvarado, Breakdown of the Korringa Law of Nuclear Spin Relaxation in Metallic GaAs, Phys. Rev. Lett. **109**, 086601 (2012).

[15] Y. S. Chen, J. Huang, A. Ludwig, D. Reuter, A. D. Wieck, and G. Bacher, Manipulation of nuclear spin dynamics in n-GaAs using an on-chip microcoil, J. Appl. Phys. **109**, 016106 (2011).

[16] F. Heisterkamp, E. Kirstein, A. Greilich, E. A. Zhukov, T. Kazimierczuk, D. R. Yakovlev, A. Pawlis, and M. Bayer, Dynamics of nuclear spin polarization induced and detected by coherently precessing electron spins in fluorine-doped ZnSe, Phys. Rev. B **93**, 081409(R) (2016).

[17] E. Evers, T. Kazimierczuk, F. Mertens, D. R. Yakovlev, G. Karczewski, T. Wojtowicz, J. Kossut, M. Bayer, and A. Greilich, Nuclear spin dynamics influenced and detected by electron spin polarization in CdTe/(Cd, Mg)Te quantum wells, Phys. Rev. B **99**, 045303 (2019).

[18] A. Abragam, *The Principles of Nuclear Magnetism* (Oxford University Press, Oxford, 1961).

[19] M. I. D'yakonov and V. I. Perel', Optical orientation in a system of electrons and lattice nuclei in semiconductors, Sov. Phys. JETP **38**, 177 (1974).

[20] *Optical Orientation*, edited by F. Meier and B. P. Zakharchenya (Elsevier, Amsterdam, 1984).

[21] J. Iafrate, Applied physics Ph.D. dissertation, University of Michigan, 2020.

[22] E. A. Zhukov, A. Greilich, D. R. Yakovlev, K. V. Kavokin, I. A. Yugova, O. A. Yugov, D. Suter, G. Karczewski, T. Wojtowicz, J. Kossut, V. V. Petrov, Yu. K. Dolgikh, A. Pawlis, and M. Bayer, All-optical NMR in semiconductors provided by resonant cooling of nuclear spins interacting with electrons in the resonant spin amplification regime, Phys. Rev. B **90**, 085311 (2014).

[23] E. Evers, N. E. Kopteva, I. A. Yugova, D. R. Yakovlev, M. Bayer, and A. Greilich, Shielding of external magnetic field by dynamic nuclear polarization in (In, Ga)As quantum dots, Phys. Rev. B **104**, 075302 (2021).